

# Asteroseismology of the Hyades with K2: first detection of main-sequence solar-like oscillations in an open cluster

Mikkel N. Lund<sup>1,2\*</sup>, Sarbani Basu<sup>3</sup>, Víctor Silva Aguirre<sup>2</sup>, William J. Chaplin<sup>1,2</sup>, Aldo M. Serenelli<sup>4</sup>, Rafael A. García<sup>5</sup>, David W. Latham<sup>6</sup>, Luca Casagrande<sup>7</sup>, Allyson Bieryla<sup>6</sup>, Guy R. Davies<sup>1,2</sup>, Lucas S. Viani<sup>3</sup>, Lars A. Buchhave<sup>8</sup>, Andrea Miglio<sup>1,2</sup>, David R. Soderblom<sup>9</sup>, Jeff A. Valenti<sup>9</sup>, Robert P. Stefanik<sup>6</sup>, and Rasmus Handberg<sup>2</sup>

<sup>1</sup>*School of Physics and Astronomy, University of Birmingham, Edgbaston, Birmingham, B15 2TT, UK*

<sup>2</sup>*Stellar Astrophysics Centre, Department of Physics and Astronomy, Aarhus University, Ny Munkegade 120, DK-8000 Aarhus C, Denmark*

<sup>3</sup>*Department of Astronomy, Yale University, PO Box 208101, New Haven, CT 06520-8101, USA*

<sup>4</sup>*Institute of Space Sciences (CSIC-IEEC), Campus UAB, Carrer de Can Magrans, s/n E-08193 Cerdanyola del Vallès (Barcelona), Spain*

<sup>5</sup>*Laboratoire AIM, CEA/DRF - CNRS - Univ. Paris Diderot - IRFU/SaP, Centre de Saclay, 91191 Gif-sur-Yvette Cedex, France*

<sup>6</sup>*Harvard-Smithsonian Center for Astrophysics, 60 Garden Street Cambridge, MA 02138 USA*

<sup>7</sup>*Research School of Astronomy and Astrophysics, Mount Stromlo Observatory, The Australian National University, ACT 2611, Australia*

<sup>8</sup>*Centre for Star and Planet Formation, Natural History Museum of Denmark & Niels Bohr Institute, University of Copenhagen, Øster Voldgade 5-7, DK-1350 Copenhagen K, Denmark*

<sup>9</sup>*Space Telescope Science Institute, 3700 San Martin Drive, Baltimore, MD 21218, USA*

Accepted 2016 August 24. Received on 2016 August 23; in original form 2016 April 7

## ABSTRACT

The Hyades open cluster was targeted during Campaign 4 (C4) of the NASA K2 mission, and short-cadence data were collected on a number of cool main-sequence stars. Here, we report results on two F-type stars that show detectable oscillations of a quality that allows asteroseismic analyses to be performed. These are the first ever detections of solar-like oscillations in main-sequence stars in an open cluster.

**Key words:** Asteroseismology — methods: data analysis — galaxies: star clusters: individual: Hyades — stars: rotation — stars: individual: EPIC 210444167 (HIP 20357, vB 37); EPIC 210499243 (HIP 19877, vB 20)

## 1 INTRODUCTION

The Hyades is one of the youngest and closest open clusters to our solar system; its close proximity of only  $\sim 47$  pc means that it has been extensively studied, and serves as an important benchmark for distances in our Galaxy (see Perryman et al. 1998, for a review). Because of its youth (with an isochrone-based age estimated to be around 550 – 625 Myr) it contains many rapidly rotating stars whose rotation rates can be readily determined, hence it is commonly used as an anchor in calibrating gyrochronology relations which link rotation rates to stellar ages.

Asteroseismology — the study of stellar oscillations — offers independent measures of stellar properties. Results from the *Kepler* mission have shown the power of asteroseismology in relation to characterisation and age dating of both field and cluster stars (Gilliland et al. 2010; Basu et al. 2011; Stello et al. 2011; Miglio

et al. 2012; Chaplin et al. 2014; Silva Aguirre et al. 2015). Regrettably, the nominal *Kepler* mission did not observe nearby clusters, but K2, the repurposed *Kepler* mission (Howell et al. 2014), will allow us to study many interesting clusters. In this Letter we present the first asteroseismic analysis of main-sequence (MS) stars in the Hyades, specifically two MS solar-like oscillators. We note in passing that White et al. (in prep.) from K2 observations, and Beck et al. (2015) from a ground-based campaign, have detected oscillations in three Hyades red-giants.

The development of the paper proceeds as follows: In Section 2 we discuss the reduction of K2 data. We also describe the other known properties of the targets and present a set of new radial velocity data designed to confirm cluster membership and identify short-period binaries, and introduce in Section 3 the spectroscopic analysis of the stars. In Section 4.1 we discuss how the asteroseismic data were used to determine stellar parameters. In Section 4.2 we present our analysis of the signatures of rotation; the seismic modelling is presented in Section 4.3, with distance estimates using the

\* E-mail: lundm@bison.ph.bham.ac.uk

asteroseismic properties being compared to other distance indicators in Section 4.4. We end with a discussion of our findings in Section 5.

## 2 DATA

The Hyades open cluster, seen in the constellation of Taurus, was observed in short-cadence (SC;  $\Delta t \approx 1$  min) during Campaign 4 (C4) of the K2 mission. SC data were collected for a total of 14 targets in the Hyades region.

Light curves were extracted from background-corrected pixel data<sup>1</sup> using the K2P<sup>2</sup> pipeline (Lund et al. 2015). Briefly, K2P<sup>2</sup> defines pixel masks for targets in a given frame by using an unsupervised clustering algorithm on pixels above a given flux threshold. Subsequently, an image segmentation algorithm is run on each pixel-cluster to adjust the pixel mask should two or more targets happen to fall within it. The light curves were rectified using a modified version of the KASOC filter (Handberg & Lund 2014) to remove trends from the apparent motion of the targets on the CCD and other instrumental signatures. Power density spectra were created using a least-squares sine-wave fitting method, normalised by the RMS-scaled version of Parseval’s theorem (see Kjeldsen 1992; Frandsen et al. 1995).

We searched the power spectra of all observed stars for indications of seismic excess power — two targets were identified, EPIC 210444167 and 210499243; from here on we will refer to these as E167 and E243. Based on proper motion and radial velocity studies by, e.g., Schwan (1991), Perryman et al. (1998), and de Bruijne, Hoogerwerf & de Zeeuw (2001) both targets are members of the Hyades. In Figure 1 we show the power spectra for the targets. The stars have spectral types F5 IV-V (E167; Gray, Napier & Winkler 2001) and F5 V (E243; Gebran et al. 2010).

The star E243 has been studied before. E243 was specifically highlighted in de Bruijne, Hoogerwerf & de Zeeuw (2001) for lying above the Hyades main-sequence ( $\Delta V \sim 0.07$  mag), and it was speculated if stellar variability or activity could be responsible for this, but at that time a good estimate of the rotational velocity was unavailable. In the Catalog of Components of Double and Multiple stars (CCDM; Dommanget & Nys 2002)<sup>2</sup> the star (A) is listed with two secondary components (B and C), both with magnitudes in the range  $V \sim 11.5$  — this multiplicity would give a change of ( $\Delta V \sim 0.02$  mag). We note, however, that the components listed in the CCDM are at very large separations of  $137.5''$  (AB) and  $151.4''$  (AC), corresponding to  $\sim 35$  and  $\sim 39$  pixels on the *Kepler* CCD. The B component (Ba) has itself a faint companion (Bb), and the C component is a spectroscopic binary. From proper motions, radial velocity (RV) data from the Harvard-Smithsonian Center for Astrophysics (CfA), and colours neither Ba, Bb, nor C are associated with E243 or the Hyades cluster. Neither of these targets fall within the assigned pixel mask of E243, and the photometry for E243 A is thus unaffected by B and C. E243 was furthermore found to be a single system from an analysis of speckle images by Patience et al. (1998); this does not necessarily, however, rule out a very close companion within the  $0''.05$  confusion limit of the speckle analysis.

Radial velocities can provide additional constraints on the possibility that close unresolved companions are contaminating the

light of E167 and E243. Both stars have been monitored for more than 35 years using RV instruments at CfA, and both appear to be single-lined, with no direct evidence for light from a companion. The velocities for E167 appear to be constant, but there is suggestive evidence for acceleration in a long-period spectroscopic orbit for E243 (Figure A1). There is insufficient information to put a strong constraint on the possible light contamination from a faint companion to E243, but a contribution of several percent cannot be ruled out. Four instruments have been used for the CfA velocities reported here for the first time (see Appendix A): three almost identical versions of the CfA Digital Speedometers (Latham 1992) on the 1.5-m Wyeth Reflector at the Oak Ridge Observatory in the Town of Harvard, Massachusetts, and on the MMT and 1.5-m Tillinghast Reflector at the Fred Lawrence Whipple Observatory on Mount Hopkins, Arizona; and more recently the Tillinghast Reflector Echelle Spectrograph (TRES; Szentgyorgyi & Fűrész 2007; Fűrész 2008), a modern fiber-fed CCD echelle spectrograph on Mount Hopkins. Both stars show substantial line broadening due to rotation,  $\sim 22$  km s<sup>-1</sup> for E167 and  $\sim 67$  km s<sup>-1</sup> for E243, so the line profiles are heavily oversampled at the instrumental resolutions of about 6.7 km s<sup>-1</sup>. Velocities were derived using the most appropriate rotationally broadened templates from the CfA library of synthetic spectra and are reported here on the native CfA system, which is about 0.14 km s<sup>-1</sup> more negative than the IAU system. Thus 0.14 km s<sup>-1</sup> should be added to the velocities reported in Table A1 and plotted in Figure A1 to put them onto the IAU system. Mean radial velocities in the IAU system of  $38.80 \pm 0.63$  km s<sup>-1</sup> (E167) and  $39.87 \pm 1.83$  km s<sup>-1</sup> (E243) are obtained, where the uncertainties are given by the root-mean-square (RMS) values of the individual velocities. These mean velocities agree well with the mean radial velocity of  $39.42 \pm 0.36$  km s<sup>-1</sup> derived by Madsen, Dravins & Lindegren (2002) for the Hyades from a moving-cluster analysis, and thus stipulate to the Hyades membership of the stars.

There are a few additional historical velocities for E167 and E243 in the literature, extending the time coverage to 82 and 101 years, respectively. Unfortunately the precision for the earliest velocities is poor and the systematic offset of the zero points is not well established. The historical velocities do strengthen the impression that E167 has been constant, and the velocity of E243 was lower 100 years ago.

## 3 ATMOSPHERIC AND STELLAR PARAMETERS

We have obtained spectroscopic parameters for the targets from several sources: (1) Values are available from the Geneva-Copenhagen Survey (GCS; Nordström et al. 2004) in their re-derived version by Casagrande et al. (2011); (2) Spectroscopic data were collected using the TRES spectrograph on the 1.5-m Tillinghast telescope at the F. L. Whipple Observatory; atmospheric parameters were derived using the Stellar Parameter Classification pipeline (SPC; Buchhave et al. 2012). Following Torres et al. (2012) we added in quadrature uncertainties of 59 K and 0.062 dex to the  $T_{\text{eff}}$  and [M/H] from SPC; (3) We also estimated  $T_{\text{eff}}$  using the Infra-Red Flux Method (IRFM; Casagrande et al. 2014). This method also gives a measure of the stellar angular diameter  $\theta$  which combined with the parallax provides an independent estimate of the stellar radius (Silva Aguirre et al. 2012). A reddening of  $E(B - V) = 0.003 \pm 0.002$  (Taylor 1980) was adopted for the IRFM derivation. Reddening was neglected in the derivation of the GCS values, but the low value for  $E(B - V)$  has virtually no impact on the derived stellar parameters. Final SPC parameters

<sup>1</sup> downloaded from the KASOC database; [www.kasoc.phys.au.dk](http://www.kasoc.phys.au.dk)

<sup>2</sup> CCDM J04158+1525A/WDS J04158+1524A (WDS; The Washington Double Star Catalog, Mason et al. 2001)

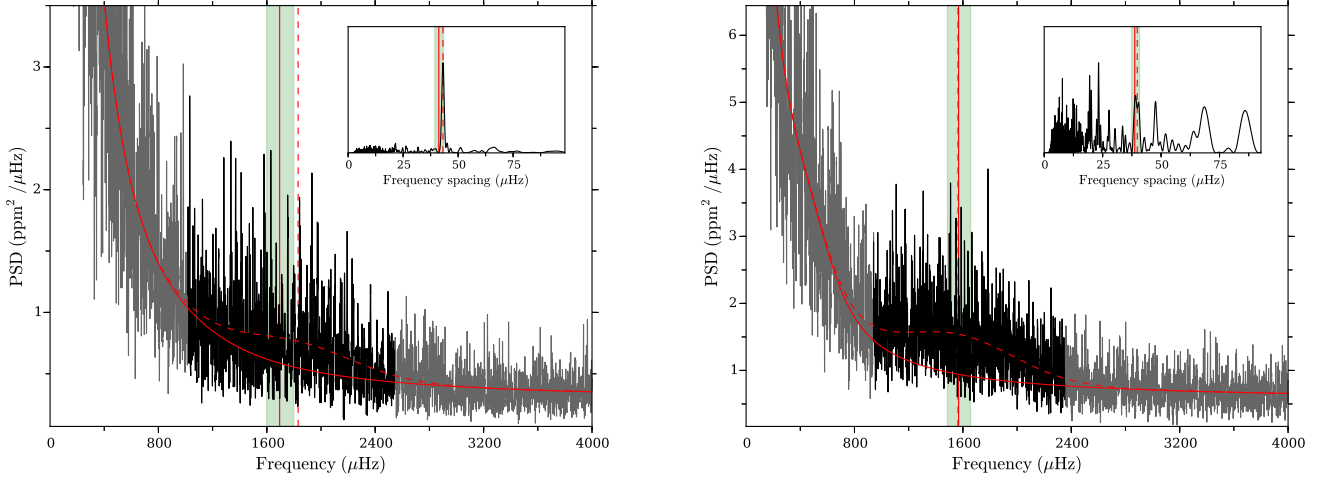


**Figure 1.** Power density spectra of E167 (left) and E243 (right), smoothed by a  $3\mu\text{Hz}$  Epanechnikov filter. The inserts show power-of-power spectra ( $\text{PS} \otimes \text{PS}$ ) from the region of the power spectra in black. The (full) vertical red lines indicate the spectroscopically estimated values for  $\nu_{\text{max}}$  of  $1695 \pm 100\mu\text{Hz}$  (E167) and  $1568 \pm 86\mu\text{Hz}$  (E243), with uncertainties given by the shaded green region; the corresponding lines in the  $\text{PS} \otimes \text{PS}$  inserts give the expected values for  $\Delta\nu/2$  from these  $\nu_{\text{max}}$  estimates following Huber et al. (2011). Dashed vertical lines indicate the measured values for  $\nu_{\text{max}}$  and  $\Delta\nu$  (see Section 4.1). The full red lines show the obtained fits to the granulation backgrounds, with the red dashed line showing the fitted Gaussian envelope used to estimate  $\nu_{\text{max}}$ .

were obtained after iterating with a  $\log g$  fixed at the asteroseismic value determined from  $\nu_{\text{max}}$  and  $T_{\text{eff}}$  from  $g \propto \nu_{\text{max}} \sqrt{T_{\text{eff}}}$ , and with a fixed metallicity of  $[\text{M}/\text{H}] = 0.164 \pm 0.08$ . The metallicity is obtained from the average of the recent spectroscopic analysis results of Hyades members by Liu et al. (2016). We note that the adopted value from Liu et al. (2016) agrees well, within the adopted uncertainty of 0.08 dex, with previous average estimates from, for instance, Cayrel, Cayrel de Strobel & Campbell (1985); Boesgaard & Budge (1988); Boesgaard & Friel (1990); Perryman et al. (1998); Paulson, Sneden & Cochran (2003); Takeda et al. (2013); and Dutra-Ferreira et al. (2016). A fixed metallicity was adopted because the SPC pipeline has difficulties with stars with a value of  $v \sin i_*$  as high as that inferred for E243 (Table 1); this is because high rotation leads to rotational broadening that might cause blending of lines. The overall agreement between the different parameter sets does, however, lend credibility to the SPC values. Final parameters are given in Table 1 —  $T_{\text{eff}}$  and  $[\text{M}/\text{H}]$  will serve as constraints in the asteroseismic modelling presented in Section 4.3.

From the spectroscopic parameters we can predict values for  $\nu_{\text{max}}$  using scaling relations (Kjeldsen & Bedding 1995). Masses were estimated from the IRFM  $T_{\text{eff}}$  via the Hyades isochrone from Pinsonneault et al. (2004), radii from  $L$  and  $T_{\text{eff}}$ , and using  $\nu_{\text{max},\odot} = 3090 \pm 30\mu\text{Hz}$ , and  $T_{\text{eff},\odot} = 5777\text{ K}$  (Huber et al. 2011; Chaplin et al. 2014). In Figure 1 the estimates are seen to agree well with the seismic power excess and the measured values of  $\nu_{\text{max}}$ . For the above prediction we estimated luminosities from kinematically improved parallaxes by Madsen, Dravins & Lindegren (2002) and V-band magnitudes from Joner et al. (2006). The relations of Flower (1996) as presented in Torres (2010) were used for the bolometric correction. Such a comparison is valuable, because it allows us a check of our predictions against the estimated seismic observables, and thus our ability to securely propose targets for future K2 campaigns.

## 4 ANALYSIS

### 4.1 Asteroseismic parameter estimation

We first determined the global asteroseismic properties  $\Delta\nu$  and  $\nu_{\text{max}}$ . Here  $\Delta\nu$  is defined as the frequency spacing between consecutive radial orders ( $n$ ) of modes with a given angular degree ( $l$ ), and  $\nu_{\text{max}}$  as the frequency where the modes show their maximum amplitudes. To estimate  $\nu_{\text{max}}$  we fit the stellar noise background following the procedure described in Lund et al. (2014). For the background we adopt a model given by a sum of power laws with free exponents, one for each phenomenon contributing to the background (see, e. g., Kallinger et al. 2014, and references therein), and include a Gaussian envelope to account for the power excess from oscillations. The obtained background fits are shown in Figure 1. We estimate  $\Delta\nu$  from fit of a squared Gaussian function including a background to a narrow range of the power-of-power spectrum ( $\text{PS} \otimes \text{PS}$ ) centred on the  $\Delta\nu/2$  peak. We note that the small frequency separation  $\delta\nu_{02}$  — given by the frequency difference between adjacent  $l = 0$  and  $l = 2$  modes as  $\delta\nu_{02} = \nu_{n,0} - \nu_{n-1,2}$  — could not be estimated from the data. See Table 1 for extracted parameters. The extracted values for  $\nu_{\text{max}}$  and  $\Delta\nu$  agree within uncertainties with the  $\Delta\nu \propto \nu_{\text{max}}^\alpha$  scaling by Huber et al. (2011).

In Figure 2 we show the background corrected échelle diagram (Grec, Fossat & Pomerantz 1983) for E167, smoothed to a resolution of  $10\mu\text{Hz}$ . Over-plotted is the scaled échelle diagram (see Bedding & Kjeldsen 2010) of frequencies for KIC 3733735<sup>3</sup>, which in terms of fundamental parameters is similar to E167, especially the similar age estimated at  $800 \pm 400\text{ Myr}$  (Chaplin et al. 2014). It is noteworthy how well the structure in the ridges of KIC 3733735 match that of E167, which indicates that the targets are indeed very similar. KIC 3733735, which is also a fast rotator, has been studied in relation to activity and rotation by Mathur et al. (2014a) and Keifer et al. (2016; submitted). The ridge identification from this scaling matches that obtained using the  $\epsilon$ -method by White et al. (2011).

<sup>3</sup> a.k.a. *Shere-Khan* in the KASC working group 1 CAtalogue.

**Table 1.** Spectroscopic parameters and common identifications for Hyades targets with detected oscillations. We give values obtained from the Stellar Parameter Classification pipeline (SPC; Buchhave et al. 2012), the Geneva-Copenhagen Survey (GCS; Nordström et al. 2004) in their re-derived version by Casagrande et al. (2011), and the InfraRed Flux Method (IRFM; see Casagrande et al. 2014). Angular diameters ( $\theta$ ) are from the IRFM. Systematic uncertainties of 59 K and 0.062 dex were added in quadrature to the SPC  $T_{\text{eff}}$  and  $[M/H]$  following Torres et al. (2012). We have highlighted in bold face the measured seismic values of  $\Delta\nu$  and  $\nu_{\text{max}}$ . SPC values were iterated with a log  $g$  fixed to the seismic estimate and a fixed metallicity of  $[M/H] = 0.164$  (Liu et al. 2016).

| EPIC                   | HIP   | HD    | Kp<br>(mag) | $\theta$<br>(mas) | $\nu_{\text{max}}$<br>( $\mu\text{Hz}$ ) | $\Delta\nu$<br>( $\mu\text{Hz}$ ) | Source             | $T_{\text{eff}}$<br>(K)                          | $[M/H]$<br>(dex)          | log $g$<br>(cgs; dex)  | $v \sin i_*$<br>( $\text{km s}^{-1}$ ) |
|------------------------|-------|-------|-------------|-------------------|--|-----------------------------------|--------------------|--|---------------------------|------------------------|--|
| 210444167 <sup>a</sup> | 20357 | 27561 | 6.545       | $0.296 \pm 0.008$ | <b><math>1831 \pm 47</math></b>          | <b><math>86.2 \pm 1.5</math></b>  | SPC<br>GCS<br>IRFM | $6761 \pm 77$<br>$6695 \pm 102$<br>$6711 \pm 81$ | $0.164 \pm 0.080$<br>0.07 | $4.24 \pm 0.1$<br>4.15 | $22.0 \pm 0.5$                         |
| 210499243 <sup>b</sup> | 19877 | 26911 | 6.264       | $0.331 \pm 0.010$ | <b><math>1564 \pm 58</math></b>          | <b><math>79.6 \pm 2.0</math></b>  | SPC<br>GCS<br>IRFM | $6901 \pm 77$<br>$6765 \pm 80$<br>$6771 \pm 81$  | $0.164 \pm 0.080$<br>0.17 | $4.18 \pm 0.1$<br>4.18 | $66.8 \pm 0.5$                         |

<sup>a</sup>Also known as CI Melotte 25 37, vB 37; <sup>b</sup>also known as 48 Tau, V1099 Tau, HR 1319, CI Melotte 25 20, vB 20.

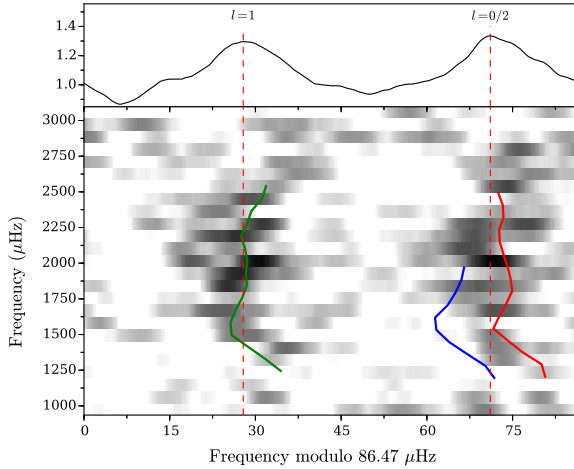


**Figure 2.** Grey scale échelle diagram for E167, smoothed horizontally to a resolution of  $10 \mu\text{Hz}$ . The lines show the frequency-ridges of KIC 3733735 (red  $l = 0$ ; green  $l = 1$ ; blue  $l = 2$ ) after multiplying by 0.9361 and forcing (by eye) the  $\epsilon$  to match that of E167 by shifting the ridges by  $6 \mu\text{Hz}$ . The top panel shows the vertically collapsed échelle giving the combined signal of the ridges.

The determination of  $\Delta\nu$  for E243 is more uncertain than that for E167, as also seen from the PS  $\otimes$  PS in Figure 1. We believe the reason for this can be found in the combination of the rotation rate, which for both stars is high, and stellar inclination — as described in Section 4.2 below, E167 is likely seen at a low inclination angle, while E243 seems to be observed edge-on. For E167 this would greatly decrease the visibility of rotationally split ( $m \neq 0$ ) mode components, leaving with highest visibility the zonal ( $m = 0$ ) components (Gizon & Solanki 2003). First of all, this would explain the distinguishable ridges in the échelle diagram (Figure 2). Additionally, the value of  $\delta_{01} \approx 0 \mu\text{Hz}$  obtained from the ridge averages shown in Figure 2 explains the strong signal in the PS  $\otimes$  PS at  $\Delta\nu/2$  — with  $\delta_{01}$  given as the offset of  $l = 1$  modes from the midpoint between the surrounding  $l = 0$  modes, i. e.,  $\delta_{01} = \frac{1}{2}(\nu_{n,0} + \nu_{n+1,0}) - \nu_{n,1}$  (see, e. g., Bedding 2011). On the other hand, the  $i_* \approx 90^\circ$  configuration for E243 would maximise the rotational confusion of the power spectrum, and the difficulty in extracting  $\Delta\nu$ . Concerning the estimation of  $\Delta\nu$  we tested the effect of adding rotation on the PS  $\otimes$  PS and found that this had a negligible impact on the central position of the  $\Delta\nu$  and  $\Delta\nu/2$  peaks, and this both from an inclination of  $i_* = 0^\circ$  and  $90^\circ$ . The main effect observed was a change in the relative heights between the peaks. This suggests that that PS  $\otimes$  PS provides a robust estimate of  $\Delta\nu$  even in the case of high rotation, in agreement with Mosser & Appourchaux (2009)

who obtained good  $\Delta\nu$  estimates for some fast rotators observed by CoRoT (Mosser et al. 2009). We checked for needed line-of-sight corrections to  $\nu_{\text{max}}$  following Davies et al. (2014) — For E167 this amounts to  $\delta\nu_s \approx 0.23 \mu\text{Hz}$  at  $\nu_{\text{max}}$ ; for E243  $\delta\nu_s \approx 0.19 \mu\text{Hz}$ , both well within our adopted uncertainties on  $\nu_{\text{max}}$ .

## 4.2 Rotation

We were unable to obtain a good estimate of the stellar rotation from the rotational splittings of mode frequencies. The surface rotation could, however, be studied using K2 light curves, which show signs of spot modulation. We estimated the surface rotation period in three complimentary ways (Aigrain et al. 2015), namely, from the imprint in the power spectrum at low frequencies (see, e. g., Nielsen et al. 2013), from the autocorrelation function (ACF) (see, e. g., McQuillan, Aigrain & Mazeh 2013), and from a Morlet wavelet analysis of the light curve (see Mathur et al. 2010; García et al. 2014; Ceillier et al. 2016). All three methods agree for both stars. In Figure 3 we show the ACFs of the light curves where only the correction from the apparent movement on the CCD has been removed, i. e., any long term trends will be retained.

For E167 we see the presence of two periodicities (see Figure 3), viz.,  $\sim 0.8$  and  $\sim 7$  days. Which of these periodicities represent the rotation is somewhat ambiguous, but from the wavelet analysis the  $\sim 0.8$  day period is favoured. In the fast scenario ( $P_{\text{rot}} \approx 0.8$  days) the star would rotate at about  $\sim 18\%$  of break-up<sup>4</sup> and have an inclination of  $\sim 14 \pm 2^\circ$ . Concerning the projected rotation rate used to obtain the inclination Mermilliod, Mayor & Udry (2009) gives an independent and corroborating value of  $v \sin i_* = 20.4 \pm 2.0 \text{ km s}^{-1}$ . The longer period signal might be interpreted as the effect of beating of close frequencies from differential rotation — indeed, signal is seen in the power spectrum in a group of peaks at  $\sim 13.8 \mu\text{Hz}$  ( $\sim 0.84$  days), at  $\sim 28.8 \mu\text{Hz}$  (close to sum of grouped peaks), and at  $\sim 0.6$ – $1.6 \mu\text{Hz}$  (close to differences of grouped peaks) as would be expected for a beating signal (see, e. g., Mathur et al. 2014a). Removing the  $\sim 7$  day signal from the ACF we obtain a spot decay time of  $\sim 10$  days (see McQuillan, Aigrain & Mazeh 2013, their Figure 4). In terms of  $(B - V)_0$ , or mass, the fast scenario is supported by the proximity to the Kraft break (Kraft 1967), which marks where the surface convection zone becomes too shallow to produce a significant braking through a magnetised wind and the observed rotation rate thus becomes highly dependent on the initial rotation rate (see, e. g., van Saders & Pinsonneault 2013). Given that we see solar-like oscillations and possible signals from spots

<sup>4</sup> computed as  $v_{\text{crit}} \approx \sqrt{2GM/3R_p}$  and assuming that the polar radii  $R_p$  can be approximated by the non-rotating radius (Maeder 2009).



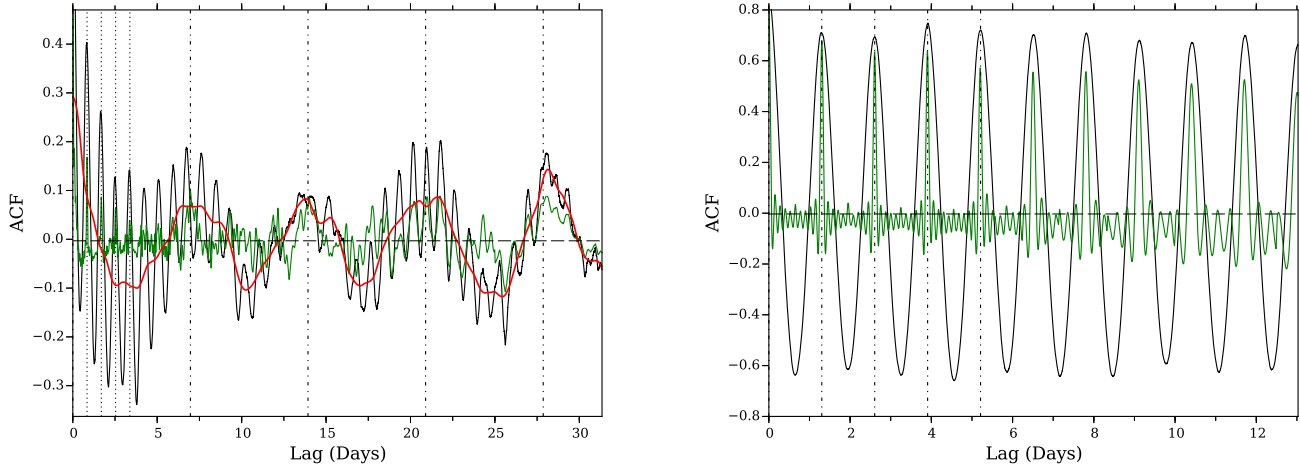


**Figure 3.** Autocorrelation functions for E167 (left) and E243 (right), where only the systematics from the apparent stellar motion on the CCD and a 30 day Epanechnikov (Hastie, Tibshirani & Friedman 2009) filter have been removed. Vertical broken lines indicate the first four maxima of a given periodicity. For E167 we have in red added a 1.23 day Epanechnikov smoothed version to highlight the underlying  $\sim 7$  day periodicity. In green we shown the so-called narrowed autocorrelation (NACF) where the response at a given lag is formed from the mean of 10 equally spaced lags of the ACF (Brown & Puckette 1989; Brown & Zhang 1991). The narrow peaks in the NACF is a testament to the strong regularity in and stability of the periodic signals.

the star must have a convective envelope, but given the relatively young age of the star (compared to its MS lifetime) it is conceivable that spin-down has not had time to take effect. The slow scenario of  $P_{\text{rot}} \approx 7$  days matches the rotation period of  $P_{\text{rot}} \approx 6$  days predicted from the  $P_{\text{rot}} - (J - K_s)$  relation for the Hyades by Delorme et al. (2011), but we note that the  $(J - K_s)$  colour of our target is at the limit of the calibration for this relation. In terms of other gyrochronology relations from, for instance, Barnes (2007) and Mamajek & Hillenbrand (2008) the fast scenario is supported.

If the rotation rate follows the fast scenario higher order effects should perturb the oscillation frequencies (see, e.g., Kjeldsen et al. 1998; Reese, Lignières & Rieutord 2006; Ouazzani & Goupil 2012). Suárez et al. (2010) describe the effect on the ridges of the échelle diagram from including rotation in a perturbative manner and near-degeneracy effects, and find among other effects a shift in the  $\delta_{01}$  spacing between ridges. As mentioned in Section 4.1 we find  $\delta_{01} \approx 0 \mu\text{Hz}$  from the ridge averages shown in Figure 2; from a range of models matching the star in terms of mass, age, and metallicity we derive a median  $\delta_{01} \approx 2.3 \pm 0.6 \mu\text{Hz}$ , where the uncertainty is given by the median-absolute-deviation of the individual model values. This difference could potentially be caused by rotation, but an in-depth analysis of such higher order effects is beyond the scope of the current paper.

For E243 only a single period of  $\sim 1.28$  days is seen in the ACF (right panel of Figure 3), which corresponds to  $\sim 12\%$  of break-up. Comparing the measured  $v \sin i_*$  to the estimated rotational velocity suggests that the star is seen at an angle of  $i_* \approx 90^\circ$ , that is, edge-on. Concerning the projected rotation rate used to obtain the inclination Gunn & Kraft (1963), Kraft (1965), and Hoffleit & Jaschek (1982) (see Hoffleit & Warren 1995), give independent and largely corroborating values of  $v \sin i_* = 50, 55$ , and  $53 \text{ km s}^{-1}$ . E243 was studied by Krisciunas et al. (1995) in a search for  $\gamma$ -Doradus Type variables in the Hyades, where the authors postulate that the detected variability is likely due to spot modulation<sup>5</sup>. Curiously, these

authors find a periodicity of 1.4336 days, albeit from only 76 data points over a 20 day period.

An additional assessment of the stellar activity signal comes with the measured coronal activity in terms of X-ray luminosity. From the *ROSAT* X-ray hardness ratio measurements in the 0.1 – 2.4 keV band by Voges et al. (1999) we obtained for E167 an X-ray to bolometric luminosity of  $\log_{10} R_X = -4.82 \pm 0.08$ , with  $R_X = L_X/L_{\text{bol}}$ . Here we used the conversion between *ROSAT* counts and hardness ratio to flux by Fleming et al. (1995) and Schmitt, Fleming & Giampapa (1995), and the luminosity estimated in Section 3. The above value corresponds largely to those from the 0.2 – 2.8 keV band *Einstein Observatory* and *ROSAT* All-Sky Survey (RASS) measurements by, respectively, Stern et al. (1981) and Stern, Schmitt & Kahabka (1995) after converting when appropriate to the *ROSAT* 0.1 – 2.4 keV band using PIMMS<sup>6</sup>. For E243 we derive from measurements by Voges et al. (1999) a value of  $\log_{10} R_X \approx -5.47 \pm 0.16$ ; Coronal X-ray measurements from the RASS by Huensch, Schmitt & Voges (1998) and *ROSAT* measurements from Stern, Schmitt & Kahabka (1995) largely agree with this estimate. Wright et al. (2011) offers a relation between  $R_X$  and the Rossby  $Ro$  number (see also Pizzolati et al. 2003; Douglas et al. 2014), where  $Ro$  is defined as  $P_{\text{rot}}/\tau_c$  with  $\tau_c$  being the mass-dependent convective turnover time-scale. In the following we use the  $\tau_c(M)$  relation from Wright et al. (2011) to determine  $Ro$ , with the mass from the seismic modelling (Section 4.3).

For E167 the two different scenarios for the rotation rate corresponds to Rossby numbers of  $Ro \sim 0.10 \pm 0.01$  (fast) and  $Ro \sim 0.83 \pm 0.06$  (slow). From Wright et al. (2011) one should for  $Ro \sim 0.83$  expect a level of  $R_X \approx -5.18 \pm 0.24$ , and for  $Ro \sim 0.10$  the star should fall in the saturated regime with  $\log_{10} R_X \approx -3.13 \pm 0.08$ . For E243 one would expect a value of  $\log_{10} R_X \approx -3.38 \pm 0.28$ . As seen the measured levels disagree with those expected for E243 and the fast scenario for E167. The  $(B - V)$  colours of the stars, with values of  $(B - V) = 0.42$  (E167) and  $(B - V) = 0.41$  (E243), do, however, also place the stars outside the calibration range adopted by

<sup>5</sup> according to the SIMBAD database this study is the reason why the star is listed in Samus, Durlevich & et al. (2009) (and hence SIMBAD) as an ellipsoidal variable star, which it is not.

<sup>6</sup> The Chandra Portable Interactive Multi-Mission Simulator, [www.cxc.harvard.edu/toolkit/pimms.jsp](http://www.cxc.harvard.edu/toolkit/pimms.jsp)

Wright et al. (2011). Comparing instead to Vilhu & Walter (1987) who include hotter stars we find that the two stars conform with an expected range of  $R_X \approx -4.5$  to  $-5.5$ . The relatively low levels of chromospheric activity also agrees with the results of Simon & Landsman (1991) and Schrijver (1993), who both include E243 in their analysis. These authors find that activity is reduced for stars earlier than  $\sim F5$ , likely due to an inefficient dynamo operating in the shallow convection zone of such early-type stars. In a study of F5-type stars in the Hyades Böhm-Vitense et al. (2002) finds that  $(B - V) \approx 0.42 - 0.43$  marks a transition region in the dependence of X-ray flux with  $v \sin i_*$  (with a decreasing X-ray flux with increasing  $v \sin i_*$ ), and in the onset of an efficient magnetic braking. Both stars thus seem to be in a very interesting region in terms of rotation and activity.

For both stars we further assessed the mean activity level using the activity proxy  $\langle S_{\text{ph},k=5} \rangle$  as defined in García et al. (2010) and Mathur et al. (2014a,b). For E167 we adopted the fast scenario for the period used in calculating the activity proxy. We obtained values of  $\langle S_{\text{ph},k=5} \rangle = 273 \pm 6$  ppm (E167) and  $\langle S_{\text{ph},k=5} \rangle = 249 \pm 7$  ppm (E243). Comparing these with García et al. (2014, their Figure 10) it is clear that the two stars occupy a region of the  $P_{\text{rot}} - \langle S_{\text{ph},k=5} \rangle$  space that is unexplored with data from the nominal mission — this likely stems from the sparsity in the number of young, hot, stars that were suggested for observations for the sake of detecting solar-like oscillations.

### 4.3 Asteroseismic modelling

The two targets analysed here only provide us with limited seismic information, that is, only the average seismic parameters  $\Delta\nu$  and  $\nu_{\text{max}}$ . These were used together with estimates of the two stars' metallicity and effective temperatures to determine the global parameters of the stars using grid based searches. Three pipelines were used in the modelling — the Yale-Birmingham pipeline (YB; Basu, Chaplin & Elsworth 2010; Basu et al. 2012; Gai et al. 2011), the Bellaterra Stellar Parameters Pipeline (BeSPP; Serenelli et al. 2013, Serenelli (in prep.)), and the Bayesian Stellar Algorithm pipeline (BASTA; Silva Aguirre et al. 2015). Three different grids of models were used in the case of YB, with models from the Dartmouth group (Dotter et al. 2008), the Yonsei-Yale ( $Y^2$ ) isochrones (Demarque et al. 2004), and the Yale Stellar Evolution Code (YREC; Demarque et al. 2008) as described by Basu et al. (2012) (YREC2). In all cases  $\Delta\nu$  for the YB models were calculated using the simple scaling relation between  $\Delta\nu$  and density (i.e.,  $\Delta\nu \propto \sqrt{M/R^3}$ ). BeSPP and BASTA used grids of models calculated using the Garching Stellar Evolution Code (GARSTEC; Weiss & Schlattl 2008). For BeSPP and BASTA model values for  $\Delta\nu$  were calculated using both the scaling relation and individual frequencies of radial modes. In cases where the  $\Delta\nu$  scaling relation was used, the corrections given in White et al. (2011) (for YB) and Serenelli et al. (2016, in prep.) (for BeSPP and BASTA) were applied to correct for the deviations of  $\Delta\nu$  values from the usual scaling relations. The value of  $\nu_{\text{max}}$  was computed using the usual scaling relation ( $\nu_{\text{max}} \propto g/\sqrt{T_{\text{eff}}}$ ). Further details of the pipelines, grids, and scaling relations are described in Chaplin et al. (2014) and Silva Aguirre et al. (2015).

From the grid-based modelling (GBM) we obtain for E167 values of  $M = 1.41 \pm 0.06 M_{\odot}$ ,  $R = 1.48 \pm 0.03 R_{\odot}$ ,  $\rho = 0.60 \pm 0.15 \text{ g cm}^{-3}$ , and  $t = 1020 \pm 387 \text{ Myr}$ ; for E243 we obtain  $M = 1.47 \pm 0.06 M_{\odot}$ ,  $R = 1.61 \pm 0.03 R_{\odot}$ ,  $\rho = 0.50 \pm 0.13 \text{ g cm}^{-3}$ , and  $t = 1132 \pm 304 \text{ Myr}$ . The reported values are those obtained from the BASTA pipeline using the SPC  $T_{\text{eff}}$  and  $[\text{Fe}/\text{H}]$ . We have

added in quadrature to the formal uncertainties a systematic uncertainty given by the root-mean-square difference between the reported BASTA values and those obtained from the other pipelines and spectroscopic inputs.

Both grid-based age estimates are seen to be slightly higher than those normally derived from isochrone fitting to the full colour-magnitude diagram (CMD). This difference is not completely unexpected, and has its origins in the limited nature of the data available to us here, as we now go on to explain. Nevertheless, as we shall also see, including the asteroseismic parameters for these main-sequence stars gives much better constraints on the fundamental properties than would be possible from CMD fitting of main-sequence stars alone.

We begin by recalling that CMD fitting of clusters works well only when data are available that span a range of evolutionary states, i.e. including turn-off stars and also red-giant-branch stars. The left-hand panel of Figure 4 shows the CMD of the Hyades using data from Stern, Schmitt & Kahabka (1995). The plotted isochrones are from GARSTEC, with colour indicating age (see the sidebar) and linestyle indicating metallicity (full-line isochrones have  $[\text{Fe}/\text{H}] = 0.2$ , while dashed-line isochrones have  $[\text{Fe}/\text{H}] = 0.15$ ). The distance modulus adopted for this plot (and subsequent analysis) was  $(m - M) = 3.25$ . We used  $E(B - V) = 0.003 \pm 0.002$  (Taylor 1980) and  $R_V \equiv A_V/E(B - V) = 3.1$  to de-redden the values from Stern, Schmitt & Kahabka (1995). Note that the two stars with asteroseismic detections are plotted in red (here using updated colours from Jones et al. (2006)).

We used the BeSPP pipeline to fit the observed CMD data in Figure 4 to the GARSTEC isochrones. The right-hand panels show the resulting  $\chi^2$  surfaces for two fits: one where we limited data to the main-sequence only ( $6 < V < 11$ , right) and another where we used all the available data (stars with  $V < 11$ , left). For both cases shown we adopted  $[\text{Fe}/\text{H}] = 0.2$ . We see that limiting to the main-sequence only provides no discernible constraint on age. The constraints are of course even weaker if we perform CMD fits using the two asteroseismic stars only (again with no seismic data). In contrast, we obtain good constraints on the age, and optimal values that agree with the canonical literature values, when we include targets beyond the main-sequence (see also Perryman et al. 1998 and Pinsonneault et al. 2004). Unfortunately, stars close to the turn off are likely to be too hot to show solar-like oscillations. Nevertheless, we see that the asteroseismic results obtained on the two stars — albeit using average asteroseismic parameters only — give much better constraints than those provided by the CMD fits to non-seismic data on main-sequence stars alone.

That the age constraints from the asteroseismic results are not tighter still reflects the nature of the average asteroseismic parameters. Both depend (in whole or large part) on different combinations of ratios of mass and radius — they thus lack explicit information on core properties and this has an impact on age estimates for stars in the relatively slow MS phase (Gai et al. 2011; Chaplin et al. 2014). Much tighter constraints are possible on the low-age part of the MS when using individual oscillation frequencies (Silva Aguirre et al. 2015).

Nevertheless, we still see a bias in the asteroseismic age estimates, and some of this arises from the way in which ages are estimated using a probabilistic approach when matching to isochrones (or grids) of stellar models. If a star lies equally close to two isochrones in terms of input parameters the most likely will be chosen based on evolutionary speed. Therefore, without prior knowledge, one is much more likely to find a star that belongs to an older (say over 1 Gyr) isochrone because evolution is slower than for a

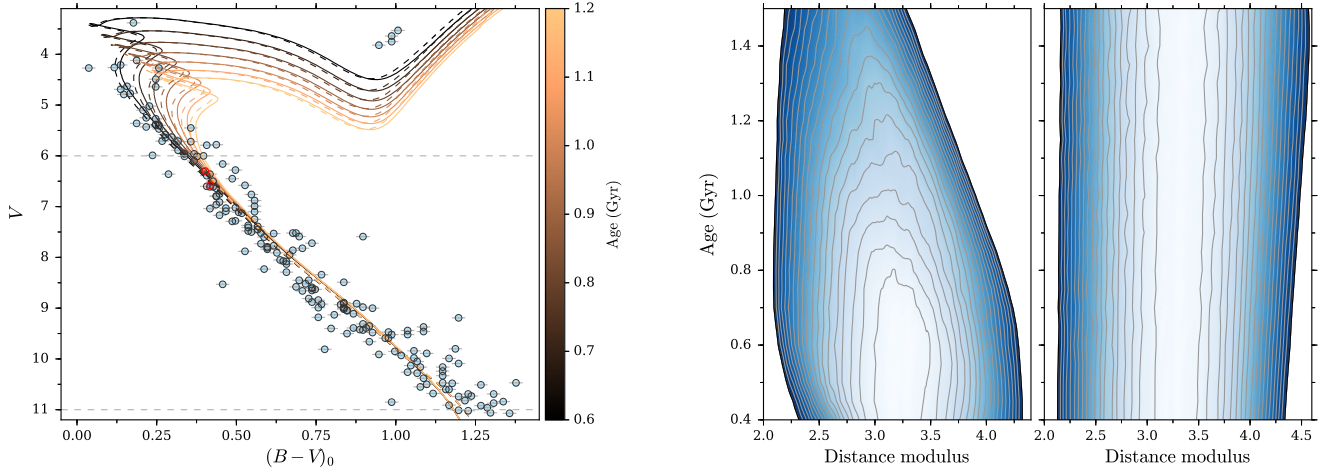


**Figure 4.** Left: colour-magnitude diagram (CMD) of Hyades stars, with parameters adopted from [Stern, Schmitt & Kahabka \(1995\)](#). The colour of the GARSTEC plotted isochrones indicate to age; full-line isochrones have  $[\text{Fe}/\text{H}] = 0.2$ , while dashed-lined ones have  $[\text{Fe}/\text{H}] = 0.15$ . For all isochrones we adopted for this plot a distance modulus of  $(m - M) = 3.25$ . We adopted  $E(B - V) = 0.003 \pm 0.002$  ([Taylor 1980](#)) and  $R_V \equiv A_V/E(B - V) = 3.1$  to de-redden the values from [Stern, Schmitt & Kahabka \(1995\)](#). The two stars analysed in this work are given by the red markers, here using updated colours from [Joner et al. \(2006\)](#). Right:  $\chi^2$  surfaces for CMD fits to stars with  $V < 11$  (left panel) and  $6 < V < 11$  (right panel) as a function of age and distance modulus, going from high  $\chi^2$ -values in dark blue to low values in light blue. For both cases shown  $[\text{Fe}/\text{H}] = 0.2$ .

sub 1-Gyr isochrone. Two of our pipelines (BASTA and BeSPP) use Bayesian schemes when computing the posterior parameter distributions, and here correct for the density of points in the adopted grids to make a proper marginalisation — this correction explicitly introduces the effect of evolutionary speed (see, e. g., [Pont & Eyer \(2004\)](#) and [Jørgensen & Lindegren \(2005\)](#) for examples and further discussion).

There are two main reasons for the bias, one easy to remove and one more fundamental. The first reason is that at low ages, the distribution function of ages for a given star cuts off abruptly at zero, biasing the result to higher ages. This effect can be mitigated to some extent by using the logarithm of the ages, but this does not remove the bias completely. The second reason for the bias is more fundamental, and has to do with the fact that on the main-sequence, stars within a small metallicity range can have many different ages for a given range of temperature and luminosity (or in the asteroseismic context a given range of  $\nu_{\text{max}}$ ). In other words, isochrones of many different ages can pass through the error-box. As described above, evolutionary speed makes it much more likely to encounter an older than a younger star, and therefore the results of any grid-based modelling will have a fundamental bias towards higher ages if no prior on age is adopted. Figure B1 shows this clearly. The bias can be reduced if effective temperature and metallicity can be measured to a much better precision. In the case of clusters, having data on more stars in different evolutionary phases of course helps greatly because we can apply the condition that all stars must have the same age, which is essentially the assumption made in determining ages by fitting isochrones to cluster colour-magnitude diagrams. There are also other factors to note. The two stars here are different to many of the stars analysed for asteroseismology in *Kepler*, in terms of being relatively hot, massive, young, and rapidly rotating. This of course raises the question of whether assumptions made regarding the mapping of the average asteroseismic parameters to stellar properties are incorrect for these stars? The results suggest there is not a significant bias. First, the relationship of  $\Delta\nu$  to  $\nu_{\text{max}}$  follows that shown by the asteroseismic cohort of *Kepler* stars. We also examined the potential impact of rotational mixing

on  $\Delta\nu$ , which is unaccounted for in the models we used, by looking at differences in stellar MESA models ([Paxton et al. 2011](#)) with and without convective core overshoot. We found no appreciable change in  $\Delta\nu$  from varying the amount of overshoot, which conforms with the results reported by [Eggenberger et al. \(2010\)](#) who studied the effect of adding rotational mixing to a  $1M_{\odot}$  model. We therefore adopt the assumption that the model values of  $\Delta\nu$  and  $\nu_{\text{max}}$  are representative of what would be found for slowly rotating stars. We also remind the reader that in Section 4.1 it was found that rotation should not affect our ability to extract a good estimate of  $\Delta\nu$ .

The above of course also goes to the issue of the physics used in our stellar models. Might missing physics be a cause of the bias? The obvious question we can answer in relation to this is whether, when we use our adopted models, we are able to recover the canonical age estimate when presented with the usual observational CMD data as input (i. e., colours and an assumed distance modulus and metallicity as input). As discussed above (Figure 4), we have demonstrated that when BeSPP is coupled to GARSTEC, we recover a satisfactory age. That does not of course say that the physics is indeed correct.

Recently, [Brandt & Huang \(2015a,b,c\)](#) performed an isochrone analysis which included rotation via the models of [Ekström et al. \(2012\)](#) and [Georgy et al. \(2013\)](#). By adding rotation, which in the adopted models had the effect of lengthening the MS lifetime, these authors find a slightly higher age than the consensus, namely,  $t \sim 750 \pm 100$  Myr. This result rests on the same handful of upper MS ( $M > 1.7M_{\odot}$ ) turn-off stars that guided the isochrone fittings by [Perryman et al. \(1998\)](#).

#### 4.4 Distances

With the seismic solution for the stellar radii and an angular diameter from the IRFM, we can estimate the seismic distance to the cluster as follows:

$$d_{\text{seis}} = C \frac{2R_{\text{seis}}}{\theta_{\text{IRFM}}}, \quad (4.1)$$

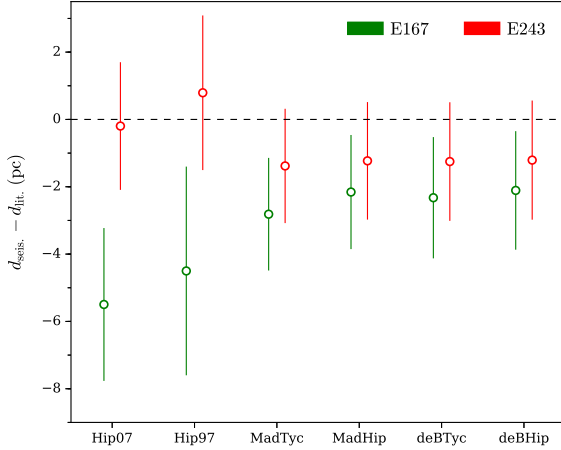


**Figure 5.** Comparison of distances obtained from the seismic radii (average from different spectroscopic inputs and pipelines) and the IRFM angular diameter with those determined from parallaxes in the literature.

where  $C$  is a conversion factor to parsec (see [Silva Aguirre et al. 2012](#); [Rodrigues et al. 2014](#)). We find seismic distances of  $d_{\text{seis}} = 46.9 \pm 1.5$  pc (E167) and  $d_{\text{seis}} = 45.2 \pm 1.6$  pc (E243). In Figure 5 we compare these to the distances derived from trigonometric parallaxes from *Hipparcos* by [van Leeuwen \(2007\)](#) (Hip07), [van Leeuwen et al. \(1997\)](#) (Hip97), those from [de Bruijne, Hoogerwerf & de Zeeuw \(2001\)](#) using secular parallaxes from Tycho-2 ([Høg et al. 2000](#)) (deBTyc) or *Hipparcos* ([van Leeuwen et al. 1997](#)) (deB-Hip), and those from [Madsen, Dravins & Lindgren \(2002\)](#) using secular parallaxes as above (MadTyc/MadHip). We find that all parallax distances for E243 match the seismic ones reasonably well; for E167 all distances are  $>1\sigma$  larger than the seismic ones.

## 5 DISCUSSION AND OUTLOOK

We have presented the asteroseismic results on two cool main-sequence stars belonging to the Hyades open cluster. These are the first ever detections of solar-like oscillations in main-sequence stars in an open cluster. Both stars are very likely fast rotators ( $P_{\text{rot}} < 2$  days), marking them out as quite different from the older, more slowly rotating cool main-sequence stars that dominated the asteroseismic cohort from the nominal *Kepler* mission.

The K2 mission is scheduled to re-observe the Hyades cluster in C13, providing an unprecedented opportunity to expand the asteroseismic cohort, potentially to stars for which we can do detailed modelling on individual frequencies (something that is very challenging for the two stars reported here). We have indicated in Figure 6 the stars from C13 for which we predict a detection of solar-like oscillations (including predicted marginal detections). The estimates of  $L$  used here were computed from *Hipparcos* parallaxes ([van Leeuwen 2007](#)), while  $T_{\text{eff}}$  values were computed from the colour- $T_{\text{eff}}$  relations of [Casagrande et al. \(2010\)](#).

Unfortunately neither of the targets analysed in this paper is predicted to lie on active silicon in C13<sup>7</sup>. We find, however, that 55 of the Hyades members from [Perryman et al. \(1998\)](#) will be on

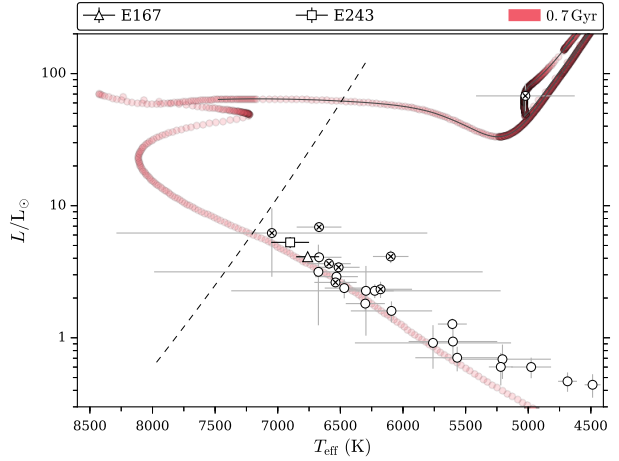


**Figure 6.** BaSTI isochrone ([Pietrinferni et al. 2004](#)) with an age of 700 Myr. For this isochrone standard BaSTI input physics was adopted, but with overshoot on the MS and with adopted heavy and Helium mass fractions of  $Z = 0.0198$  and  $Y = 0.273$ . The triangle and square symbols indicate our two targets (see legend), with  $T_{\text{eff}}$  given by the SPC and with the difference to the IRFM value added in quadrature to the uncertainty. The luminosities for the two targets are given by these  $T_{\text{eff}}$  values and the seismic radii. Circular markers indicate stars that could be observed in Campaign 13 for which we predict detectable solar-like oscillations. The stars that are further marked with a cross will be amenable to interferometric observations with PAVO@CHARA ([ten Brummelaar et al. 2005](#); [Ireland et al. 2008](#)). The dashed line gives the red edge of the classical instability strip, as defined by [Pamyatnykh \(2000\)](#). The parts of the isochrone overlaid with a solid black line indicate where  $\nu_{\text{max}}$  values computed from the standard scaling by [Kjeldsen & Bedding \(1995\)](#) drops below the long-cadence Nyquist frequency of  $\sim 283 \mu\text{Hz}$ .

silicon in C13; of these we estimate  $\sim 22$  will have *Kepler* magnitudes in the range  $K_p = 6 - 9.5$ ,  $T_{\text{eff}} \lesssim 6300$  K, and rotational periods in the range  $P_{\text{rot}} \approx 6 - 15$  days. Based on knowledge of K2 noise properties asteroseismic analysis of these targets should be feasible (see [Stello et al. 2015](#); [Van Cleve et al. 2015](#); [Lund et al., in press](#)). A joint analysis may provide constraints on the cluster age, especially if individual frequencies or even just an estimate of the core-sensitive small frequency separation  $\delta\nu_{02}$  can be obtained in some stars ([Christensen-Dalsgaard 1993](#)). Moreover, for several stars independent constraints may be obtained from interferometry with PAVO@CHARA ([ten Brummelaar et al. 2005](#); [Ireland et al. 2008](#)). One of the C13 targets is a giant and can comfortably be observed in long-cadence (LC;  $\Delta t \approx 30$  min) — this star (HIP 20885; 77 Tau) would be valuable to constrain the cluster age, especially if combined with the MS targets and the two C4 giants analysed by [White et al. \(in prep.\)](#).

## ACKNOWLEDGMENTS

We acknowledge the dedicated team behind the *Kepler* and K2 missions, without whom this work would not have been possible. We thank Daniel Huber and Benoit Mosser for useful comments on an earlier version of the paper. M.N.L. acknowledges the support of The Danish Council for Independent Research | Natural Science (Grant DFF-4181-00415). M.N.L. was partly supported by the European Community's Seventh Framework Programme (FP7/2007-2013) under grant agreement no. 312844 (SPACEINN), which is gratefully acknowledged. Funding for the Stellar Astrophysics Centre (SAC) is provided by The Danish National Research Foundation (Grant DNR106). The research was supported by the ASTERISK project

<sup>7</sup> using the K2FOV tool; [www.keplerscience.arc.nasa.gov/software.html](http://www.keplerscience.arc.nasa.gov/software.html)



(ASTERoseismic Investigations with SONG and *Kepler*) funded by the European Research Council (Grant agreement no.: 267864). W.J.C., G.R.D. and A.M. acknowledge the support of the UK Science and Technology Facilities Council (STFC). S.B. acknowledges partial support from NASA grant NNX13AE70G and NSF grant AST-1514676. A.M.S. is partially supported by grants ESP2014-56003-R and ESP2015-66134-R (MINECO). V.S.A. acknowledges support from VILLUM FONDEN (research grant 10118). R.A.G. acknowledges the support from the ANR program IDEE (n. ANR-12-BS05-0008) and the CNES. D.W.L. acknowledges partial support from the *Kepler* mission under Cooperative Agreement NNX13AB58B with the Smithsonian Astrophysical Observatory. This research has made use of the Washington Double Star Catalog maintained at the U.S. Naval Observatory; the WEBDA database, operated at the Department of Theoretical Physics and Astrophysics of the Masaryk University; and the SIMBAD database, operated at CDS, Strasbourg, France.

## References

- Aigrain S. et al., 2015, MNRAS, 450, 3211  
 Barnes S. A., 2007, ApJ, 669, 1167  
 Basu S., Chaplin W. J., Elsworth Y., 2010, ApJ, 710, 1596  
 Basu S. et al., 2011, ApJL, 729, L10  
 Basu S., Verner G. A., Chaplin W. J., Elsworth Y., 2012, ApJ, 746, 76  
 Beck P. G. et al., 2015, A&A, 573, A138  
 Bedding T. R., 2011, arXiv: 1107.1723  
 Bedding T. R., Kjeldsen H., 2010, CoAst, 161, 3  
 Boesgaard A. M., Budge K. G., 1988, ApJ, 332, 410  
 Boesgaard A. M., Friel E. D., 1990, ApJ, 351, 467  
 Böhm-Vitense E., Robinson R., Carpenter K., Mena-Werth J., 2002, ApJ, 569, 941  
 Brandt T. D., Huang C. X., 2015a, ApJ, 807, 24  
 Brandt T. D., Huang C. X., 2015b, ApJ, 807, 25  
 Brandt T. D., Huang C. X., 2015c, ApJ, 807, 58  
 Brown J. C., Puckette M. S., 1989, J. Acoust. Soc. Am., 85, 1595  
 Brown J. C., Zhang B., 1991, J. Acoust. Soc. Am., 89, 2346  
 Buchhave L. A. et al., 2012, Nature, 486, 375  
 Casagrande L., Ramírez I., Meléndez J., Bessell M., Asplund M., 2010, A&A, 512, A54  
 Casagrande L., Schönrich R., Asplund M., Cassisi S., Ramírez I., Meléndez J., Bensby T., Feltzing S., 2011, A&A, 530, A138  
 Casagrande L. et al., 2014, ApJ, 787, 110  
 Cayrel R., Cayrel de Strobel G., Campbell B., 1985, A&A, 146, 249  
 Ceillier T. et al., 2016, MNRAS, 456, 119  
 Chaplin W. J. et al., 2014, ApJS, 210, 1  
 Christensen-Dalsgaard J., 1993, in Astronomical Society of the Pacific Conference Series, Vol. 42, GONG 1992. Seismic Investigation of the Sun and Stars, Brown T. M., ed., p. 347  
 Davies G. R., Handberg R., Miglio A., Campante T. L., Chaplin W. J., Elsworth Y., 2014, MNRAS, 445, L94  
 de Bruijne J. H. J., Hoogerwerf R., de Zeeuw P. T., 2001, A&A, 367, 111  
 Delorme P., Collier Cameron A., Hebb L., Rostron J., Lister T. A., Norton A. J., Pollacco D., West R. G., 2011, MNRAS, 413, 2218  
 Demarque P., Guenther D. B., Li L. H., Mazumdar A., Straka C. W., 2008, Ap&SS, 316, 31  
 Demarque P., Woo J.-H., Kim Y.-C., Yi S. K., 2004, ApJS, 155, 667  
 Dommanget J., Nys O., 2002, VizieR Online Data Catalog, 1274, 0  
 Dotter A., Chaboyer B., Jevremović D., Kostov V., Baron E., Ferguson J. W., 2008, ApJS, 178, 89  
 Douglas S. T. et al., 2014, ApJ, 795, 161  
 Dutra-Ferreira L., Pasquini L., Smiljanic R., Porto de Mello G. F., Steffen M., 2016, A&A, 585, A75  
 Eggenberger P. et al., 2010, A&A, 519, A116  
 Ekström S. et al., 2012, A&A, 537, A146  
 Fleming T. A., Molendi S., Maccacaro T., Wolter A., 1995, ApJS, 99, 701  
 Flower P. J., 1996, ApJ, 469, 355  
 Frandsen S., Jones A., Kjeldsen H., Viskum M., Hjorth J., Andersen N. H., Thomsen B., 1995, A&A, 301, 123  
 Fűrész G., 2008, PhD thesis, Univertisy of Szeged, Hungary  
 Gai N., Basu S., Chaplin W. J., Elsworth Y., 2011, ApJ, 730, 63  
 García R. A. et al., 2014, A&A, 572, A34  
 García R. A., Mathur S., Salabert D., Ballot J., Régulo C., Metcalfe T. S., Baglin A., 2010, Science, 329, 1032  
 Gebran M., Vick M., Monier R., Fossati L., 2010, A&A, 523, A71  
 Georgy C., Ekström S., Granada A., Meynet G., Mowlavi N., Eggenberger P., Maeder A., 2013, A&A, 553, A24  
 Gilliland R. L. et al., 2010, PASP, 122, 131  
 Gizon L., Solanki S. K., 2003, ApJ, 589, 1009  
 Gray R. O., Napier M. G., Winkler L. I., 2001, AJ, 121, 2148  
 Grec G., Fossat E., Pomerantz M. A., 1983, Sol. Phys., 82, 55  
 Gunn J. E., Kraft R. P., 1963, ApJ, 137, 301  
 Handberg R., Lund M. N., 2014, MNRAS, 445, 2698  
 Hastie T., Tibshirani R., Friedman J., 2009, The Elements of Statistical Learning: Data Mining, Inference, and Prediction, Second Edition, Springer Series in Statistics. Springer Science & Business Media  
 Hoffleit D., Jaschek C., 1982, The Bright Star Catalogue. Fourth revised edition. (Containing data compiled through 1979).  
 Hoffleit D., Warren, Jr. W. H., 1995, VizieR Online Data Catalog, 5050, 0  
 Høg E. et al., 2000, A&A, 355, L27  
 Howell S. B. et al., 2014, PASP, 126, 398  
 Huber D. et al., 2011, ApJ, 743, 143  
 Huensch M., Schmitt J. H. M. M., Voges W., 1998, A&AS, 132, 155  
 Ireland M. J. et al., 2008, in SPIE Conference Series, Vol. 7013, Optical and Infrared Interferometry, p. 701324  
 Joner M. D., Taylor B. J., Laney C. D., van Wyk F., 2006, AJ, 132, 111  
 Jørgensen B. R., Lindegren L., 2005, A&A, 436, 127  
 Kallinger T. et al., 2014, A&A, 570, A41  
 Kjeldsen H., 1992, PhD thesis, University of Aarhus, Denmark, (1992)  
 Kjeldsen H., Arentoft T., Bedding T., Christensen-Dalsgaard J., Frandsen S., Thompson M. J., 1998, in ESA Special Publication, Vol. 418, Structure and Dynamics of the Interior of the Sun and Sun-like Stars, Korzennik S., ed., p. 385  
 Kjeldsen H., Bedding T. R., 1995, A&A, 293, 87  
 Kraft R. P., 1965, ApJ, 142, 681  
 Kraft R. P., 1967, ApJ, 150, 551  
 Krisciunas K., Crowe R. A., Lueddeke K. D., Roberts M., 1995, MNRAS, 277, 1404  
 Latham D. W., 1992, in Astronomical Society of the Pacific Conference Series, Vol. 32, IAU Colloq. 135: Complementary Approaches to Double and Multiple Star Research, McAlister H. A., Hartkopf W. I., eds., p. 110  
 Liu F., Yong D., Asplund M., Ramírez I., Meléndez J., 2016, MNRAS, 457, 3934  
 Lund M. N., Handberg R., Davies G. R., Chaplin W. J., Jones C. D., 2015, ApJ, 806, 30  
 Lund M. N. et al., 2014, A&A, 570, A54  
 Madsen S., Dravins D., Lindegren L., 2002, A&A, 381, 446  
 Maeder A., 2009, Physics, Formation and Evolution of Rotating Stars, Astronomy and Astrophysics Library. Springer Berlin Heidelberg  
 Mamajek E. E., Hillenbrand L. A., 2008, ApJ, 687, 1264  
 Mason B. D., Wycoff G. L., Hartkopf W. I., Douglass G. G., Worley C. E., 2001, AJ, 122, 3466  
 Mathur S. et al., 2014a, A&A, 562, A124  
 Mathur S. et al., 2010, A&A, 511, A46  
 Mathur S., Salabert D., García R. A., Ceillier T., 2014b, JSWSC, 4, A15  
 McQuillan A., Aigrain S., Mazeh T., 2013, MNRAS, 432, 1203  
 Mermilliod J.-C., Mayor M., Udry S., 2009, A&A, 498, 949  
 Miglio A. et al., 2012, MNRAS, 419, 2077  
 Mosser B., Appourchaux T., 2009, A&A, 508, 877  
 Mosser B., Baudin F., Lanza A. F., Hurlot J. C., Catala C., Baglin A., Auvergne M., 2009, A&A, 506, 245  
 Nielsen M. B., Gizon L., Schunker H., Karoff C., 2013, A&A, 557, L10  
 Nordström B. et al., 2004, A&A, 418, 989  
 Ouazzani R.-M., Goupil M.-J., 2012, A&A, 542, A99  
 Pamyatnykh A. A., 2000, in ASP Conf. Ser., Vol. 210, Delta Scuti and Related Stars, Breger M., Montgomery M., eds., p. 215

- Patience J., Ghez A. M., Reid I. N., Weinberger A. J., Matthews K., 1998, *AJ*, 115, 1972
- Paulson D. B., Sneden C., Cochran W. D., 2003, *AJ*, 125, 3185
- Paxton B., Bildsten L., Dotter A., Herwig F., Lesaffre P., Timmes F., 2011, *ApJS*, 192, 3
- Perryman M. A. C. et al., 1998, *A&A*, 331, 81
- Pietrinferni A., Cassisi S., Salaris M., Castelli F., 2004, *ApJ*, 612, 168
- Pinsonneault M. H., Terndrup D. M., Hanson R. B., Stauffer J. R., 2004, *ApJ*, 600, 946
- Pizzolato N., Maggio A., Micela G., Sciortino S., Ventura P., 2003, *A&A*, 397, 147
- Pont F., Eyer L., 2004, *MNRAS*, 351, 487
- Reese D., Lignières F., Rieutord M., 2006, *A&A*, 455, 621
- Rodrigues T. S. et al., 2014, *MNRAS*, 445, 2758
- Samus N. N., Durlevich O. V., et al., 2009, *VizieR Online Data Catalog*, 1, 2025
- Schmitt J. H. M. M., Fleming T. A., Giampapa M. S., 1995, *ApJ*, 450, 392
- Schrijver C. J., 1993, *A&A*, 269, 446
- Schwan H., 1991, *A&A*, 243, 386
- Serenelli A. M., Bergemann M., Ruchti G., Casagrande L., 2013, *MNRAS*, 429, 3645
- Silva Aguirre V. et al., 2012, *ApJ*, 757, 99
- Silva Aguirre V. et al., 2015, *MNRAS*, 452, 2127
- Simon T., Landsman W., 1991, *ApJ*, 380, 200
- Stello D. et al., 2015, *ApJL*, 809, L3
- Stello D. et al., 2011, *ApJ*, 739, 13
- Stern R. A., Schmitt J. H. M. M., Kahabka P. T., 1995, *ApJ*, 448, 683
- Stern R. A., Zolcinski M. C., Antiochos S. K., Underwood J. H., 1981, *ApJ*, 249, 647
- Suárez J. C., Goupil M. J., Reese D. R., Samadi R., Lignières F., Rieutord M., Lochard J., 2010, *ApJ*, 721, 537
- Szentgyorgyi A. H., Furész G., 2007, in *Revista Mexicana de Astronomía y Astrofísica Conference Series*, Vol. 28, *Revista Mexicana de Astronomía y Astrofísica Conference Series*, Kurtz S., ed., pp. 129–133
- Takeda Y., Honda S., Ohnishi T., Ohkubo M., Hirata R., Sadakane K., 2013, *PASJ*, 65
- Taylor B. J., 1980, *AJ*, 85, 242
- ten Brummelaar T. A. et al., 2005, *ApJ*, 628, 453
- Tonry J., Davis M., 1979, *AJ*, 84, 1511
- Torres G., 2010, *AJ*, 140, 1158
- Torres G., Fischer D. A., Sozzetti A., Buchhave L. A., Winn J. N., Holman M. J., Carter J. A., 2012, *ApJ*, 757, 161
- Van Cleve J. E. et al., 2015, *ArXiv e-prints* 1512.06162
- van Leeuwen F., 2007, *A&A*, 474, 653
- van Leeuwen F., Evans D. W., Grenon M., Grossmann V., Mignard F., Perryman M. A. C., 1997, *A&A*, 323, L61
- van Saders J. L., Pinsonneault M. H., 2013, *ApJ*, 776, 67
- Vilhu O., Walter F. M., 1987, *ApJ*, 321, 958
- Voges W. et al., 1999, *A&A*, 349, 389
- Weiss A., Schlattl H., 2008, *Ap&SS*, 316, 99
- White T. R. et al., 2011, *ApJL*, 742, L3
- Wright N. J., Drake J. J., Mamajek E. E., Henry G. W., 2011, *ApJ*, 743, 48

## APPENDIX A: RADIAL VELOCITIES FROM CFA

Table A1 gives the CfA radial velocities obtained over a period of over 35 years. The dates are given in heliocentric Julian date (minus 2400000), and the radial velocities are on the native CfA system in  $\text{km s}^{-1}$ . To put these velocities onto the IAU system, add  $0.14 \text{ km s}^{-1}$ . Concerning the estimated internal errors, these are for the CfA Digital Speedometers estimated from the anti-symmetric noise in the correlation function as described in Tonry & Davis (1979); for TRES it is an educated guess based on extensive experience with dozens of hot rapidly rotating stars. The velocities are plotted in Figure A1. See Section 2 for additional info on the data.

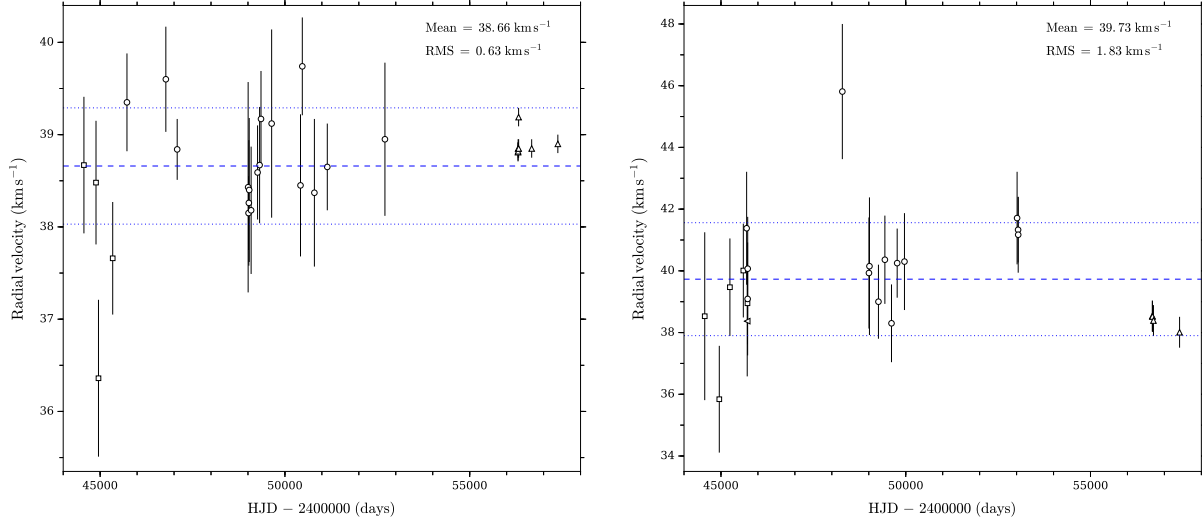
## APPENDIX B: BASTA MODEL DISTRIBUTIONS

Figure B1 Presents the posterior distributions from the GBM of E167 with BASTA. As seen from the models with an age in the interval between 500 – 800 Myr (marked in green) a higher metallicity is preferred for a good reconciliation with isochrone-based ages. The higher  $[\text{Fe}/\text{H}]$  gives a corresponding increase in  $T_{\text{eff}}$  and mass, and with it a decrease in age. It is also clear that the models that provide an age as expected for the Hyades still match the average seismic parameters for the star, indicating that these only contribute with a mild constraint on age.

**Table A1.** Radial velocity data for E167 (28 measurements) and E243 (24 measurements). The four columns give the heliocentric Julian date (minus 2400000), the radial velocity on the native CfA system in  $\text{km s}^{-1}$ , the estimated internal error, and the source of the data. To put these velocities onto the IAU system, add  $0.14 \text{ km s}^{-1}$ . For the CfA Digital Speedometers the error is estimated from the anti-symmetric noise in the correlation function as described in the [Tony & Davis \(1979\)](#); for TRES it is an educated guess based on extensive experience with dozens of hot rapidly rotating stars.

| E167                  |                              |                                       |                     | E243                  |                              |                                       |                     |
|-----------------------|------------------------------|---------------------------------------|---------------------|-----------------------|------------------------------|---------------------------------------|---------------------|
| Date<br>(HJD-2400000) | RV<br>( $\text{km s}^{-1}$ ) | Uncertainty<br>( $\text{km s}^{-1}$ ) | Source <sup>†</sup> | Date<br>(HJD-2400000) | RV<br>( $\text{km s}^{-1}$ ) | Uncertainty<br>( $\text{km s}^{-1}$ ) | Source <sup>†</sup> |
| 44560.8212            | 38.67                        | 0.74                                  | 2                   | 44560.7928            | 38.53                        | 2.72                                  | 2                   |
| 44887.8537            | 38.48                        | 0.67                                  | 2                   | 44954.7683            | 35.84                        | 1.73                                  | 2                   |
| 44954.8595            | 36.36                        | 0.85                                  | 2                   | 45241.9557            | 39.47                        | 1.58                                  | 2                   |
| 45339.8980            | 37.66                        | 0.61                                  | 2                   | 45604.9773            | 40.01                        | 1.52                                  | 2                   |
| 45725.5179            | 39.35                        | 0.53                                  | 3                   | 45694.6675            | 41.38                        | 1.83                                  | 3                   |
| 46777.6586            | 39.60                        | 0.57                                  | 3                   | 45710.5961            | 38.37                        | 1.79                                  | 1                   |
| 47084.8265            | 38.84                        | 0.33                                  | 3                   | 45717.7013            | 38.95                        | 1.33                                  | 2                   |
| 49004.6987            | 38.43                        | 1.14                                  | 3                   | 45721.6767            | 39.09                        | 1.83                                  | 3                   |
| 49015.5712            | 38.15                        | 0.40                                  | 3                   | 45723.5431            | 40.07                        | 1.68                                  | 3                   |
| 49023.6034            | 38.26                        | 0.68                                  | 3                   | 48284.6245            | 45.81                        | 2.19                                  | 3                   |
| 49033.6385            | 38.40                        | 0.78                                  | 3                   | 49004.6898            | 39.93                        | 1.80                                  | 3                   |
| 49085.5137            | 38.18                        | 0.69                                  | 3                   | 49018.5060            | 40.15                        | 2.23                                  | 3                   |
| 49259.7909            | 38.59                        | 0.51                                  | 3                   | 49261.7933            | 39.00                        | 1.20                                  | 3                   |
| 49314.8078            | 38.67                        | 0.63                                  | 3                   | 49435.5377            | 40.36                        | 1.43                                  | 3                   |
| 49352.6751            | 39.17                        | 0.52                                  | 3                   | 49614.9038            | 38.30                        | 1.26                                  | 3                   |
| 49640.8260            | 39.12                        | 1.02                                  | 3                   | 49768.5359            | 40.25                        | 1.12                                  | 3                   |
| 50421.7596            | 38.45                        | 0.77                                  | 3                   | 49965.8878            | 40.30                        | 1.57                                  | 3                   |
| 50470.5632            | 39.74                        | 0.53                                  | 3                   | 53013.6234            | 41.71                        | 1.50                                  | 3                   |
| 50797.6904            | 38.37                        | 0.80                                  | 3                   | 53040.5089            | 41.33                        | 1.06                                  | 3                   |
| 51146.7703            | 38.65                        | 0.47                                  | 3                   | 53043.5878            | 41.17                        | 1.23                                  | 3                   |
| 52706.5335            | 38.95                        | 0.83                                  | 3                   | 56673.7786            | 38.54                        | 0.50                                  | 4                   |
| 56308.7281            | 38.81                        | 0.10                                  | 4                   | 56675.8239            | 38.52                        | 0.50                                  | 4                   |
| 56309.6904            | 38.82                        | 0.10                                  | 4                   | 56703.5994            | 38.39                        | 0.50                                  | 4                   |
| 56310.7357            | 38.85                        | 0.10                                  | 4                   | 57410.7730            | 38.01                        | 0.50                                  | 4                   |
| 56323.6397            | 39.19                        | 0.10                                  | 4                   |                       |                              |                                       |                     |
| 56324.7170            | 38.85                        | 0.10                                  | 4                   |                       |                              |                                       |                     |
| 56677.6733            | 38.85                        | 0.10                                  | 4                   |                       |                              |                                       |                     |
| 57385.8825            | 38.90                        | 0.10                                  | 4                   |                       |                              |                                       |                     |

<sup>†</sup> 1: MMT Digital Speedometer; 2: Tillinghast Reflector Digital Speedometer; 3: Wyeth Reflector Digital Speedometer; 4: Tillinghast Reflector Echelle Spectrograph



**Figure A1.** Radial velocity data for E167 (left) and E243 (right) from CfA spanning a period of  $\sim 35$  years, see [Table A1](#) for the individual data values. The dashed and dotted lines indicate the mean and RMS values of the velocities, with the values given in the plots. The markers indicate the different instruments used in obtaining the data, specifically, the MMT Digital Speedometer ( $\triangleleft$ ); the Tillinghast Reflector Digital Speedometer ( $\square$ ); the Wyeth Reflector Digital Speedometer ( $\diamond$ ); the Tillinghast Reflector Echelle Spectrograph ( $\triangle$ ).

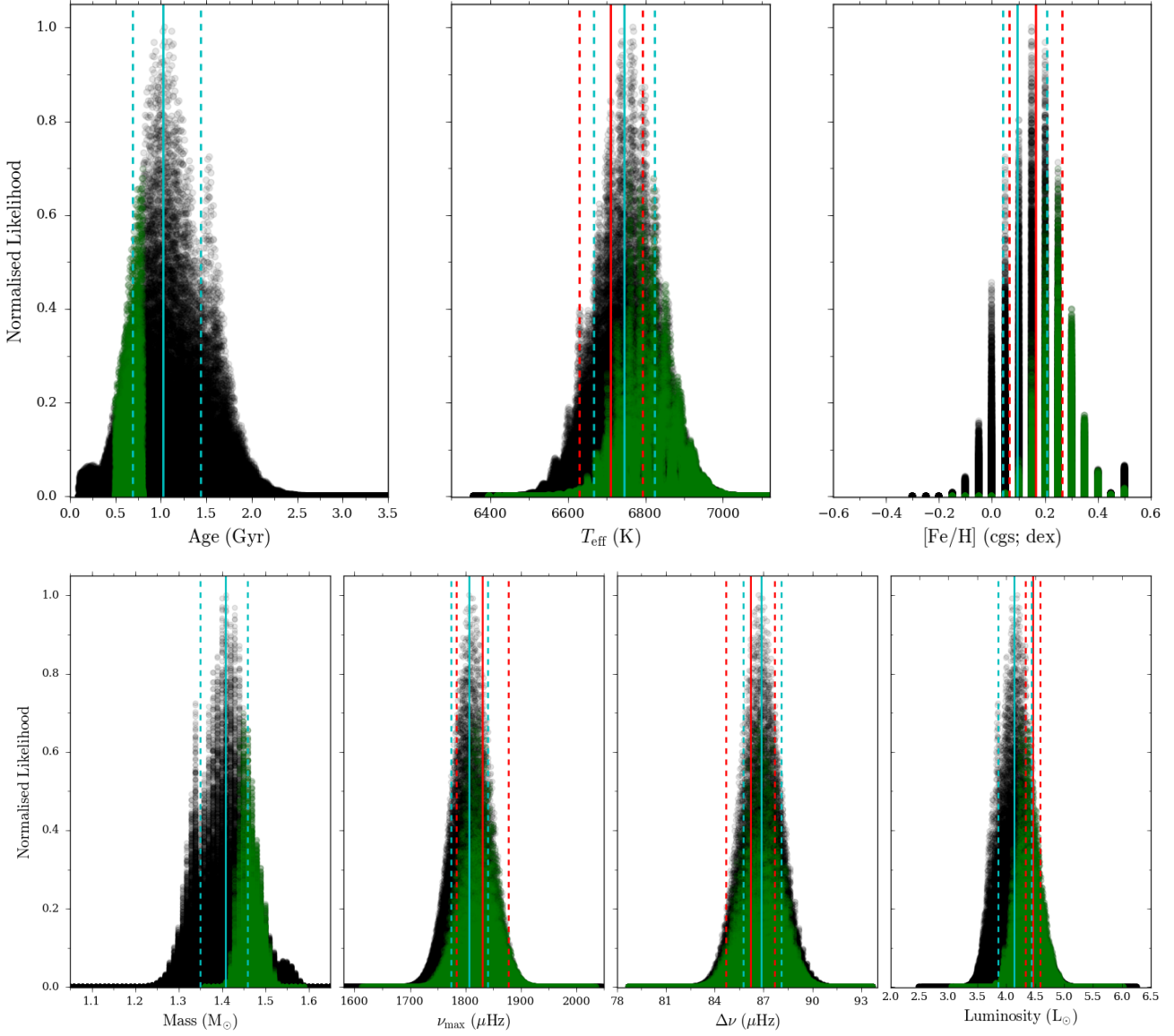


**Figure B1.** Posterior distributions from the GBM of E167 with BASTA. The different panels give the distributions for different model quantities of interest, with observed average seismic parameters and spectroscopic inputs from SPC indicated by vertical red lines, and final model values from BASTA indicated by vertical cyan lines; dashed lines indicate the  $1 - \sigma$  values on the parameters. For the luminosity the indicated value is calculated from the SPC  $T_{\text{eff}}$  and the distance from the parallax of [Madsen, Dravins & Lindegren \(2002\)](#). The models shown in green are the ones falling in the age interval between 500 – 800 Myr. In all cases likelihood values have been normalised to a maximum of 1.